Cell death monitoring using quantitative optical coherence tomography methods

Golnaz Farhat[a,b], Victor X. D. Yang[b,d], Michael C. Kolios[a,e] and Gregory J. Czarnota[a,b,c]
[a]Dept. of Medical Biophysics, University of Toronto, Toronto, Canada;
[b]Imaging Research and [c]Radiation Oncology, Sunnybrook Health Sciences Centre, Toronto, Canada;
[d]Dept. of Electrical & Computer Engineering, Ryerson University, Toronto, Canada;
[e]Dept of Physics, Ryerson University, Toronto, Canada;

ABSTRACT

Cell death is characterized by a series of predictable morphological changes, which modify the light scattering properties of cells. We present a multi-parametric approach to detecting changes in subcellular morphology related to cell death using optical coherence tomography (OCT). Optical coherence tomography data were acquired from acute myeloid leukemia (AML) cells undergoing apoptosis over a period of 48 hours. Integrated backscatter (IB) and spectral slope (SS) were computed from OCT backscatter spectra and statistical parameters were extracted from a generalized gamma (GG) distribution fit to OCT signal intensity histograms. The IB increased by 2-fold over 48 hours with significant increases observed as early as 4 hours. The SS increased in steepness by 2.5-fold with significant changes at 12 hours, while the GG parameters were sensitive to apoptotic changes at 24 to 48 hours. Histology slides indicated nuclear condensation and fragmentation at 24 hours, suggesting the late scattering changes could be related to nuclear structure. A second series of measurements from AML cells treated with cisplatin, colchicine or ionizing radiation suggested that the GG parameters could potentially differentiate between modes of cell death. Distinct cellular morphology was observed in histology slides obtained from cells treated under each condition.

Keywords: cell death, apoptosis, backscatter, optical coherence tomography, treatment monitoring, spectroscopic, envelope statistics

1. INTRODUCTION

Many cancer therapies rely on the induction of apoptosis, a form of programmed cell death, to reduce tumor burden. Cells begin to undergo apoptosis in treated tissues as early as 24 hours after the start of treatment. However, cancer treatment efficacy is still largely assessed by measuring changes in tumor size several weeks later. It has been shown with a number of cancer types that early response to therapy is indicative of overall response [1, 2]. The ability to detect early changes associated with cell death could, therefore, permit the cessation of ineffective treatments, sparing the patient from unnecessary side effects and potentially improving treatment outcome.

Apoptosis is characterized by a series of predictable morphological changes at the subcellular level. During this process, the cell undergoes a reduction in volume, disruption of the mitochondrial network, condensation and fragmentation of the nucleus and eventually fragmentation of the cell into apoptotic bodies. The structural changes that occur as a result of cell death will modify the optical and mechanical properties of tissues, which can be probed using appropriate physical techniques. We have previously used high frequency ultrasound backscatter to detect cell death both *in vitro* and in a mouse tumor model [3, 4] with the help of spectral analysis techniques developed by Lizzi *et al*. [5]. Our work demonstrated that ultrasound backscatter signals can be correlated with nuclear size [6]. In this paper we propose using optical coherence tomography (OCT) for detecting cell death. Optical coherence tomography has many advantages as an imaging modality for treatment monitoring because it is non-invasive and non-ionizing, making it safe for longitudinal studies and providing rapid imaging at low cost. Furthermore, we expect OCT to be particularly sensitive to subcellular structures because the imaging wavelengths (1.3 μm in our case) are similar in size to subcellular organelles. Light backscattered from biological tissues will undergo Mie scattering from particles and organelles inside cells, making this imaging modality sensitive to changes in size, shape and refractive index of such structures.

Biomedical Applications of Light Scattering V, edited by Adam P. Wax, Vadim Backman,
Proc. of SPIE Vol. 7907, 790713 · © 2011 SPIE · CCC code: 1605-7422/11/$18 · doi: 10.1117/12.874721

Several studies have been conducted using optical techniques to detect structural changes in cells. Light scattering methods have been applied towards detecting alterations in nuclear morphology in dysplastic cells [7] and spectroscopic OCT has been used to differentiate between cell types based on cell and nuclear morphology [8]. Optical techniques have also been applied to the detection of cell viability. Mulvey *et al.* [9] developed an elastic light scattering method for detecting changes in wavelength-dependent light scattering from cells undergoing apoptosis. Optical coherence tomography has been applied toward cell death monitoring both *in vitro* and *in vivo.* Apoptosis and necrosis have been detected in human fibroblast cells using the total attenuation coefficient of cell samples computed from OCT images [10] and changes in relative tissue scattering have been measured between viable and non-viable tissue regions in a mouse tumor model using optical frequency domain imaging [11].

We present a multi-parametric analysis technique based on both the characterization of the OCT backscattered spectrum and analysis of the intensity distribution of OCT signals obtained from an *in vitro* cell death model. This *in vitro* tumor model has been used extensively in our laboratory for cell death monitoring and provides a well-controlled environment with which we can develop our monitoring techniques [3]. In this study we demonstrate, through apoptosis time course experiments, that our method is sensitive to both early and late apoptotic changes. Furthermore, our technique shows potential for differentiating between modes of cell death through the analysis of OCT signal intensity statistics. The work here demonstrates that we can detect cell death using OCT and forms a strong foundation on which we can base future experiments *in vivo*.

2. METHODS

2.1 Biological model

Cell samples were prepared using acute myeloid leukemia cells (AML-5, Ontario Cancer Institute, Toronto, Canada). Approximately 10^9 AML cells started from frozen stock samples were grown at 37^o C in suspension flasks containing 150 mL of α-minimal essential medium supplemented with 1% streptomycin and 5% fetal bovine serum. Each cell sample was prepared from a single flask. In preparation for imaging, cells were washed with phosphate buffered saline and centrifuged in a bench top swing bucket centrifuge (Jouan CR4i, Thermo Fisher Scientific, Waltham, MA) in a flat bottom ependorff tube at 2000 *g* producing a densely packed cell pellet approximately 1 cm in diameter and 2 mm in thickness. The supernatant above the cell pellet was carefully removed using a 200 μL pipette tip. Due to its short doubling time and its non-adherent nature, this cell line permits the rapid production of large numbers of cells, as required by our model. Extensive use of AML cells in our laboratory for cell death monitoring using ultrasound techniques has allowed us to characterize the time kinetics of apoptosis and mitotic arrest in these cells. The cell packing observed in the AML cell pellets resembles that seen in tumor xenografts *in vivo* and thus, serves as a good model for cell death monitoring in tumors [12].

2.2 Cell death induction

Cell death was induced in two series of experiments. All treatments were administered to cells in suspension, prior to cell pellet preparation. The first set of experiments were designed to investigate changes in light scattering during an apoptosis time course. Apoptosis was induced by treating cells with the chemotherapeutic agent cisplatin, a DNA intercalater, which causes a p53-dependent apoptosis [13]. Seven flasks were treated simultaneously at 10 μg/mL of cisplatin and returned to the incubator for up to 48 hours with one additional untreated flask to serve as a control. Imaging times were set at 0 hours, 2 hours, 4 hours, 6 hours, 9 hours, 12 hours, 24 hours and 48 hours of cisplatin exposure. At each measurement time, a cell pellet was prepared for imaging from a single treated flask.

In the second series of experiments cells were treated with cisplatin, colchicine or ionizing radiation. Cisplatin was administered for 24 hours at the dosage described above. Colchicine is a drug that inhibits the formation of tubulin, causing the arrest of cells at metaphase in the mitotic cycle [14]. Colchicine was administered at 0.1 μg/mL for a period of 24 hours [3]. For x-ray irradiation, suspension flasks were placed in a small animal irradiator (Faxitron Cabinet X-ray system, Wheeling, IL). This system delivered 160 keV x-rays at a rate of 200cGy/min. Radiation was administered as a single fraction of 8 Gy, 24 hours prior to cells being processed for imaging. Cell samples (including the control sample) were prepared 24 hours after treatment for all cases.

2.3 Histological validation

Immediately after the completion of OCT imaging, cell pellets were fixed in 10% formalin for 48 hours and subsequently paraffin embedded and processed for haematoxylin and eosin (H&E) staining. Microscopy was carried out using a Leica DM LB microscope and digital images were acquired with the Leica DC 200 digital imaging system (Leica Microsystems GmbH, Germany). Digital images obtained from H&E sections were used to observe cell and nuclear structure.

2.4 Reference phantom

An optical scattering phantom was used as a reference for normalizing all signals measured from cell samples to maintain consistency between experiments and to remove systematic errors. The optical phantom was prepared from a silicon base mixed with titanium dioxide as the scattering agent, at a concentration of 0.1 g/mL. Reference measurements were collected at each data acquisition to remove system effects.

2.5 OCT system

Optical coherence tomography images and data were acquired using a Thorlabs Inc. (Newton, NJ) swept source OCT (OCM1300SS) system. This system uses a frequency swept external cavity laser with a central wavelength of 1325 nm and a -3 dB bandwidth of approximately 100 nm with an axial resolution of 9 µm. The mean beam spot size in the focal plane is 15 µm and the average output power of the system is 10 mW. The Thorlabs Swept source Optical Coherence Tomography Microscope software package (version 1.3.0.0, Thorlabs Inc.) was used for data acquisition.

2.6 Data acquisition and analysis

Data were acquired in the form of 14-bit OCT interference fringe signals. For each cell sample (including the reference phantom) two-dimensional (2D) data sets containing 128 axial scans were collected in 10 planes spaced at least 10 µm apart. Each 2D scan covered a total transverse distance of 1 mm. All samples were imaged such that the surface was located at the same distance in relation to the focal plane to maintain consistency between measurements with respect to variations in signal intensity due to the focal properties of the lens and the depth-dependent signal roll-off of the laser source.

As shown in figure 1(a), from each 2D scan a region of interest (ROI) covering a depth of 250 µm and a lateral distance of 780 µm was selected for analysis. The lateral dimension was chosen to give approximately 100 a-lines per b-mode image. The axial dimension was chosen to coincide with the depth of focus of the system and begins at approximately 30 µm below the cell sample surface to avoid any specular reflections.

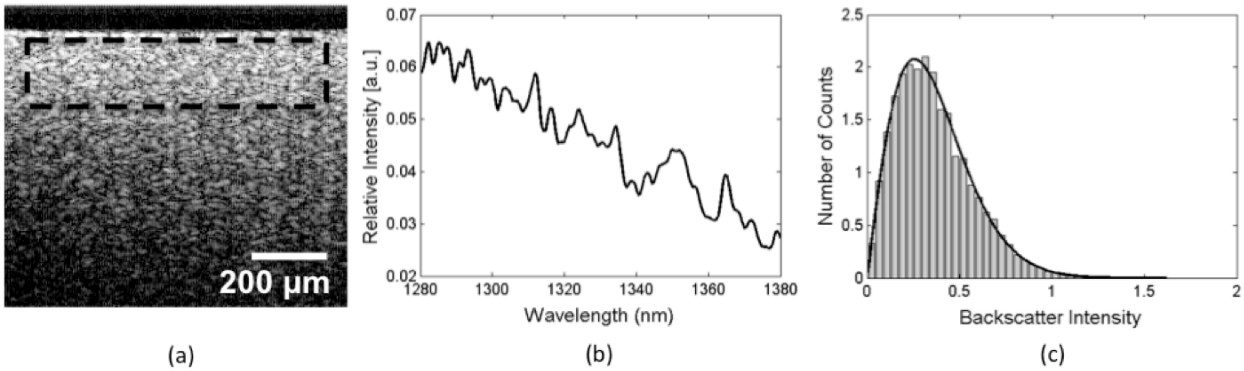

Figure 1. Analysis methods. (a) An OCT image of a cell pellet. The region of interest selected for quantitative analysis is highlighted by the dashed line. (b) Representative normalized backscatter spectrum from AML cells. (c) Signal intensity histogram (gray bars) obtained from an AML cell sample and the corresponding generalized gamma fit (solid black line).

Normalized backscatter power spectra were obtained from individual a-lines by calculating the Fourier transform of the corresponding complex interference signals and normalizing the squared magnitude of these spectra by the power spectrum computed from the titanium dioxide reference phantom. The resulting normalized power spectra (see example in figure 1(b)) were individually integrated over the -3 dB bandwidth of the light source to calculate the integrated backscatter (IB). An average IB value was computed for each 2D ROI. Within the same -3 dB bandwidth region, a linear regression was performed to fit the normalized spectra to a line, from which the spectral slope (SS) was obtained.

In order to measure the general statistics of the intensity distributions in the OCT images, a histogram of the magnitude of the acquired interference signals for each 2D ROI was calculated. Statistical parameters were obtained using an implementation of a maximum likelihood estimation routine to fit a generalized gamma probability distribution to the histograms [15] (figure 1(c)). The GG distribution is described by the following formula [16]:

$$p(r) = \frac{cr^{cv-1}}{a^{cv}\Gamma(v)} e^{-\left(\frac{r}{a}\right)^c} \quad (1)$$

In this distribution, r is the signal envelope amplitude and a, c and v are the three fitting parameters. The a parameter is related to the scale of the distribution, while the c and v parameters are related to the position of the left and right tails of the curve.

A set of average parameters was calculated for each ROI and the estimated error was calculated as a standard deviation of each of the parameters over the 10 ROIs acquired. Statistical significance for all parameters was determined using a two tailed student t-test ($p < 0.05$) for each treated sample with respect to the control sample and is indicated by an asterisk next to each point on all graphs.

3. RESULTS AND DISCUSSION

3.1 Apoptosis time course experiments

Representative H&E stained sections (figure 2) obtained from AML cell samples indicated significant structural changes after 24 hours of cisplatin exposure. Nuclear condensation and fragmentation were observed as well as irregular cell shapes indicative of cell membrane blebbing and fragmentation. These structural variations were in contrast to the morphology observed in untreated samples (0 hours) where the cells exhibited a rounded shape with the nucleus occupying the majority of the cell volume. Integrated backscatter and SS values from two experiments conducted at separate times are plotted in figure 3. The cells in both experiments were obtained from the same frozen stock, however the experiments were conducted after different lengths of time in culture indicated by the passage numbers, passage 3 (P3) and passage 7 (P7). Cells in P7 were in culture approximately 4 weeks longer than those in P3.

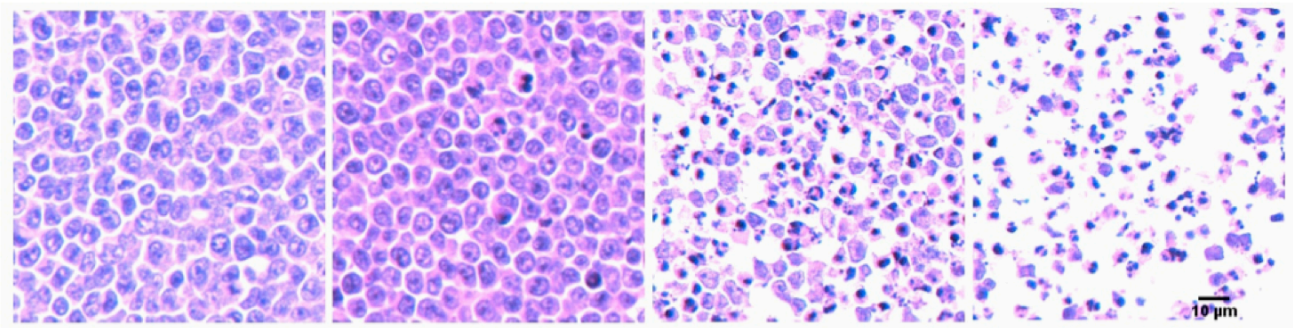

Figure 2. Representative H & E stained sections obtained from cisplatin treated cells after (a) 0 hours, (b) 12 hours, (c) 24 hours and (d) 48 hours of treatment.

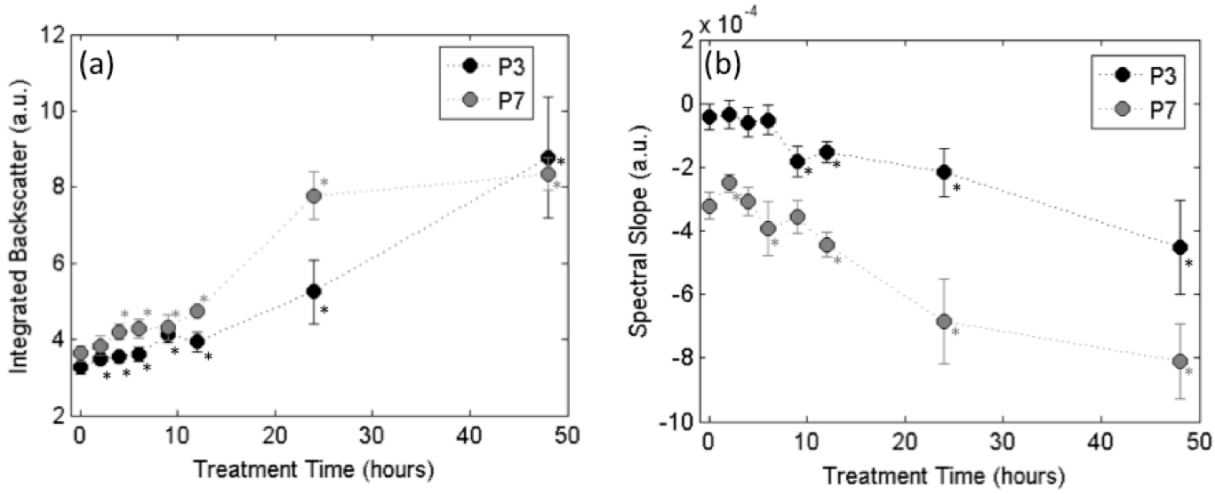

Figure 3. Spectral parameters calculated from cisplatin treated cells. (a) Integrated backscatter and (b) spectral slope. Statistical significance of parameters measured at each time point (relative to the 0 hour measurement) is indicated by an asterisk.

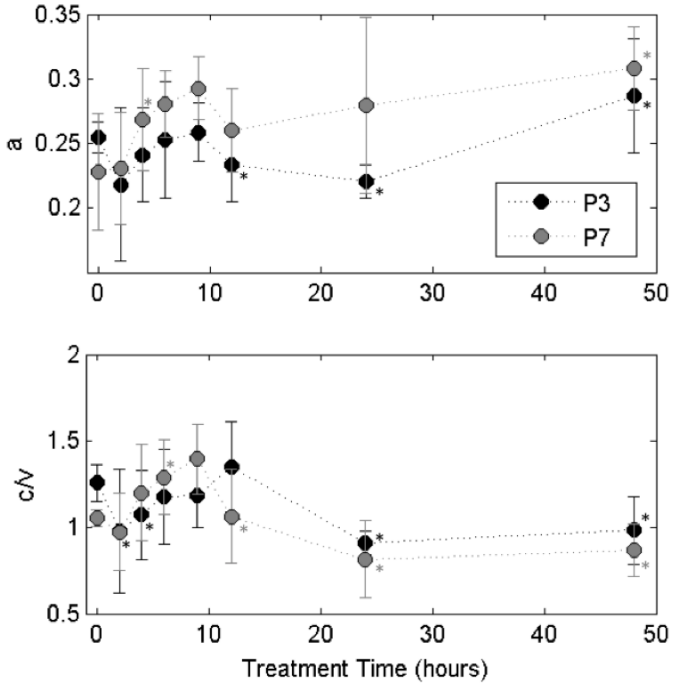

Figure 4. Generalize gamma parameters for an apoptosis timecourse experiment. (a) *a* parameter and (b) *c/v* ratio. Statistical significance of parameters measured at each time point (relative to the 0 hour measurement) is indicated by an asterisk.

Integrated backscatter values increased consistently with treatment duration, more than doubling by 48 hours with statistically significant changes observed as early as 4 hours after the start of treatment. Spectral slope decreased (increased in steepness) by 2.5-fold over 48 hours. Here significant changes were observed after 12 hours of cisplatin exposure. Generalized gamma parameters are plotted in figure 4. A slight rise and subsequent fall were seen in both sets of parameters for both series of measurements between 0 hours and 12 hours. However, due to the large variability in measurements, these changes at early times were not statistically significant. At later times the *a* parameter increased significantly after 48 hours and the *c/v* ratio decreased after 24 hours.

Between the multiple parameters extracted from the OCT data, the IB appeared to be the most robust measurement. This parameter exhibited the least amount of variability between the two cell cultures and indicated the earliest sensitivity to apoptosis with a significant increase as early as 4 hours after cisplatin exposure. Integrated backscatter is a measure of overall backscatter intensity and is related to the scattering cross-section of the cell sample. The spectral slope measurements indicated repeatability in trend, with both cell cultures exhibiting a decrease in spectral slope over 48 hours. However, we observed a significant difference between SS values for cells in P3 versus those in P7. This indicates that SS may be more sensitive to the biological variability between cell cultures. Based on Mie theory, for a given wavelength range and scattering angle the shape of the backscattered spectrum will be determined by the size and relative refractive index of the scatterers. Consequently the SS will depend on scatterer size. We expect a change in slope with apoptosis due to the fragmentation of organelles such as mitochondria and nuclei. In an elastic light scattering spectroscopy study by Mulvey et al. [9], a decrease in the negative slope of the backscatter spectrum in the 500 nm to 750 nm wavelength region was correlated with an overall decrease in dominant scatterer size. Spectral characteristics vary from one wavelength range to another; therefore, we would not necessarily expect to the SS to change in a similar way at 1300nm. Further investigation of how a decrease in scatterer size is related to the spectral slope changes we observe with apoptotic AML cells is required.

The GG parameters also indicated good repeatability in trends observed over 48 hours, despite the fact that the changes at early times were not statistical significant (based on a student t-test). The increase and decrease of both the *a* parameter and the *c/v* ratio at early times demonstrated the potential sensitivity of this analysis to early apoptotic changes. Based on this apoptosis time course analysis, however, this measurement showed reliable sensitivity only after 48 hours of treatment for the *a* parameter and after 24 hours for the *c/v* ratio.

Apoptosis is a dynamic process with time kinetics that can vary significantly between cell types, treatment types and even different batches of cells from the same cell line. The time course experiment allowed us to observe the time kinetics of this process and to correlate changes observed in our measurements with the various stages of apoptosis. For all parameters examined, small changes occurred at the early time points (2-12 hours after treatment). It is known that one of the first morphological changes observed during apoptosis is the fragmentation and deterioration of the mitochondrial network [17]. We suspect that the early changes observed in the IB parameter could be related to mitochondrial fragmentation. The most significant changes in the parameters were observed 24-48 hours after treatment. The H&E stained sections shown in figure 2 indicated significant changes in nuclear structure in this time period. Therefore, one can attribute part of the changes in the OCT signal to variations in nuclear structure. Several studies [18-20] have suggested that mitochondria may be one of the dominant scatterers with OCT imaging. However, light scattering techniques have also been used successfully to detect variations in nuclear size [7]. It is, therefore, reasonable to assume that the changes observed in the 24-48 hour time window could be related to nuclear structure.

The time kinetics of cisplatin-induced apoptosis are affected by the length of the cell cycle. The doubling time of AML cells is approximately 24 hours, however, as the length of time in culture immediately after thawing of the cells increases, the doubling time decreases and the cells may undergo apoptosis slightly earlier. Evidence of this is seen in figures 3 and 4 where the change in parameters was observed at a slightly earlier time with the P7 cells. Integrated backscatter increased at a faster rate, SS started to decrease at an earlier time and the GG parameters increased and decreased more rapidly for the P7 cells compared to cells at P3 (particularly the *c/v* ratio). This indicates that cell cycle dynamics cannot be ignored when developing methods for cell death monitoring and one must exercise caution when comparing studies using different cell types and different apoptosis induction mechanisms.

3.2 Comparing modes of cell death

In order to further investigate the sensitivity of the GG analysis technique, we analyzed cell samples undergoing three different modes of cell death. We selected 24 hours as our imaging time because it coincides with the cell doubling time and the time at which the most significant changes in OCT parameters were measured in the previous apoptosis time

course experiments. Representative H&E stained sections (figure 5) obtained from cell pellets indicated structural changes similar to those seen after 24 hours in the apoptosis time course experiment for the cisplatin treated cells. The colchicine treated cells exhibited large amounts of highly condensed nuclear material, as is expected from cells in mitotic arrest. In the irradiated cell sample we observed cells exhibiting signs of mitotic arrest as well as cells with fragmented nuclei. This is expected as ionizing radiation often causes a mix of mitotic catastrophe and apoptosis in cancer cells [12, 21, 22].

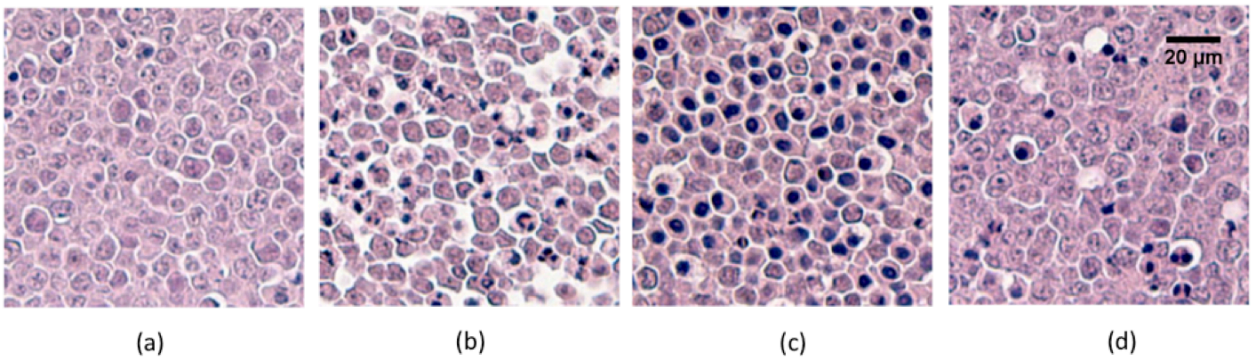

Figure 5. H&E stained sections obtained from AML cell samples, which were untreated (a), treated with cisplatin (b), colchicine (c) and 8 Gy of ionizing radiation (d).

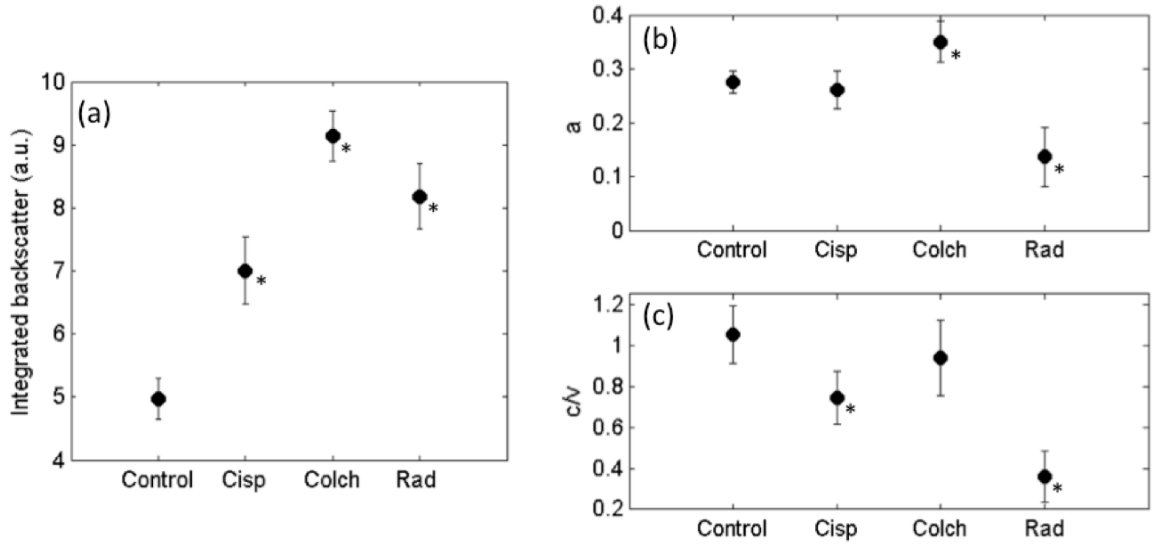

Figure 6. Calculated parameters for cell samples treated with cisplatin, colchicine or 8 Gy of ionizing radiation. (a) Integrated backscatter, (b) generalized gamma *a* parameter and (c) generalized gamma *c/v* ratio. Statistical significance of parameters measured at each time point (relative to the control measurement) is indicated by an asterisk.

Integrated backscatter (figure 6(a)) increased for all cell samples indicating that IB does not clearly differentiate between the structural changes observed in the three different modes of cell death. All changes in IB relative to the control sample were statistically significant ($p < 0.05$). If IB measurements are related to nuclear structure as we hypothesized in the previous section, it is not unexpected to see a larger increase in IB for the colchicine treated cells as they exhibit higher chromatin content.

Generalized gamma parameters are plotted in figure 6 (b) and (c). For the cisplatin treated sample we observed no significant change in *a* and a decrease in *c/v* (similar to results at 24 hours in section 3.1). An increase in the *a* and no significant change in *c/v* parameters were measured in the colchine experiments, while both parameters decreased for the radiation treated sample. From this set of experiments it appears that the GG analysis results in a unique parameter combination for each mode of cell death. These results suggest the potential for using the GG analysis as a method to differentiate between modes of cell death. They also highlight the fact that the shape and scale parameters should not be considered independently but rather as a multi-parameter measurement.

Previous work using GG analysis of signal envelope intensities with high frequency ultrasound imaging of cell pellets indicated that the *a* and *c/v* parameters may be related to scatterer number density under certain controlled conditions, while the *a* parameter may also be related to the overall backscatter intensity [23]. The relation between *a* and overall backscatter intensity does not seem to hold true for OCT. Although the IB increased for all treated cell samples, the GG *a* parameter did not. This is likely due to changes in the shape of the probability distributions. Furthermore, since it remains unclear what the dominant light scattering structures are (in terms of cellular components), it is difficult to judge the relationship between scatterer number density and the GG parameters. Currently, experiments using polystyrene microsphere phantoms are underway to better understand the effect of scatterer size and number density on the OCT signal intensity histograms.

4. CONCLUSIONS

The results described in this paper demonstrated that OCT can be used to detect apoptosis in cell pellets *in vitro*. Integrated backscatter appeared to be a robust measurement of cell death, with the ability to detect changes as early as 4 hours after treatment with cisplatin-induced apoptosis in AML cells. The spectral slope and signal envelope statistics using the generalized gamma distribution also indicated sensitivity to cell structural changes, but at later stages of apoptosis. Use of the GG analysis was further investigated by imaging cell samples under different treatment conditions and results suggested a potential for using this technique as a method to differentiate between modes of cell death. This is the first time to our knowledge that characterization of the backscatter spectrum and envelope statistics have been used on OCT data to detect cell death *in vitro*. Further investigation of the influence of scatterer size and number density is currently underway to better understand and interpret the GG analysis results.

5. REFERENCES

[1] Esteva, F. and Hortobagyi, G., "Can early response assessment guide neoadjuvant chemotherapy in early-stage breast cancer?," Journal of the National Cancer Institute, 100(8), 521 (2008).

[2] Pantaleo, M., Nannini, M., Maleddu, A., Fanti, S., Ambrosini, V., Nanni, C., Boschi, S. and Biasco, G., "Conventional and novel PET tracers for imaging in oncology in the era of molecular therapy," Cancer treatment reviews, 34(2), 103-121 (2008).

[3] Czarnota, G., Kolios, M., Abraham, J., Portnoy, M., Ottensmeyer, F., Hunt, J. and Sherar, M., "Ultrasound imaging of apoptosis: high-resolution non-invasive monitoring of programmed cell death in vitro, in situ and in vivo," British journal of cancer, 81(3), 520 (1999).

[4] Czarnota, G., Kolios, M., Vaziri, H., Benchimol, S., Ottensmeyer, F., Sherar, M. and Hunt, J., "Ultrasonic biomicroscopy of viable, dead and apoptotic cells," Ultrasound in medicine & biology, 23(6), 961-965 (1997).

[5] Lizzi, F., Feleppa, E., Kaisar Alam, S. and Deng, C., "Ultrasonic spectrum analysis for tissue evaluation," Pattern Recognition Letters, 24(4-5), 637-658 (2003).

[6] Taggart, L., Baddour, R., Giles, A., Czarnota, G. and Kolios, M., "Ultrasonic characterization of whole cells and isolated nuclei," Ultrasound in medicine & biology, 33(3), 389-401 (2007).

[7] Perelman, L., Backman, V., Wallace, M., Zonios, G., Manoharan, R., Nusrat, A., Shields, S., Seiler, M., Lima, C. and Hamano, T., "Observation of periodic fine structure in reflectance from biological tissue: a new technique for measuring nuclear size distribution," Physical Review Letters, 80(3), 627-630 (1998).

[8] Oldenburg, A., Xu, C. and Boppart, S., "Spectroscopic optical coherence tomography and microscopy," IEEE Journal of Selected Topics in Quantum Electronics, 13(6), 1629 (2007).

[9] Mulvey, C., Sherwood, C. and Bigio, I., "Wavelength-dependent backscattering measurements for quantitative real-time monitoring of apoptosis in living cells," Journal of Biomedical Optics, 14, 064013 (2009).
[10] Meer, F. J., Faber, D. J., Aalders, M. C. G., Poot, A. A., Vermes, I. and Leeuwen, T. G., "Apoptosis- and necrosis-induced changes in light attenuation measured by optical coherence tomography," Lasers Med Sci, 25(2), 259-267 (2010).
[11] Vakoc, B. J., Lanning, R. M., Tyrrell, J. A., Padera, T. P., Bartlett, L. A., Stylianopoulos, T., Munn, L. L., Tearney, G. J., Fukumura, D., Jain, R. K. and Bouma, B. E., "Three-dimensional microscopy of the tumor microenvironment in vivo using optical frequency domain imaging," Nature Medicine, 1-6 (2010).
[12] Vlad, R., [Quantitative ultrasound characterization of responses to radiotherapy in vitro and in vivo] University of Toronto, Toronto(2009).
[13] Zamble, D. and Lippard, S., "Cisplatin and DNA repair in cancer chemotherapy," Trends in biochemical sciences, 20(10), 435-439 (1995).
[14] Dustin, P., "Microtubules," American Scientific, 243, 66-76 (1995).
[15] Tunis, A., Czarnota, G., Giles, A., Sherar, M., Hunt, J. and Kolios, M., "Monitoring structural changes in cells with high-frequency ultrasound signal statistics," Ultrasound in medicine & biology, 31(8), 1041-1049 (2005).
[16] Stacy, E. W., "A Generalization of the Gamma Distribution," The Annals of Mathematical Statistics, 33(3), 6 (1962).
[17] Karbowski, M. and Youle, R., "Dynamics of mitochondrial morphology in healthy cells and during apoptosis," Cell Death & Differentiation, 10(8), 870-880 (2003).
[18] Tang, S., Sun, C., Krasieva, T., Chen, Z. and Tromberg, B., "Imaging subcellular scattering contrast by using combined optical coherence and multiphoton microscopy," Optics letters, 32(5), 503-505 (2007).
[19] Mourant, J., Canpolat, M., Brocker, C., Esponda-Ramos, O., Johnson, T., Matanock, A., Stetter, K. and Freyer, J., "Light scattering from cells: the contribution of the nucleus and the effects of proliferative status," Journal of Biomedical Optics, 5, 131 (2000).
[20] Pasternack, R. Z., JY; Boustany, NN, "Optical scatter changes at the onset of apoptosis are spatially associated with mitochondria," Journal of Biomedical Optics, 15, 040504 (2010).
[21] Dodson, H., Wheatley, S. P. and Morrison, C. G., "Involvement of centrosome amplification in radiation-induced mitotic catastrophe," Cell Cycle, 6(3), 364-70 (2007).
[22] Luce, A., Courtin, A., Levalois, C., Altmeyer-Morel, S., Romeo, P. H., Chevillard, S. and Lebeau, J., "Death receptor pathways mediate targeted and non-targeted effects of ionizing radiations in breast cancer cells," Carcinogenesis, 30(3), 432-9 (2009).
[23] Tunis, A., "Monitoring Structural Changes in Cells and Tissues with High Frequency Ultrasound Signal Statistics," Thesis, 1-98 (2005).